





RESEARCH ARTICLE | MAY 22 2024

Temperature-dependent characterization of full tensor properties of $[111]_c$ poled Mn-doped 28PIN-43PMN-29PT single crystals

Ailing Xiao; Liguang Tang  ; Guisheng Xu  ; Kechen Wu; Wenyu Luo

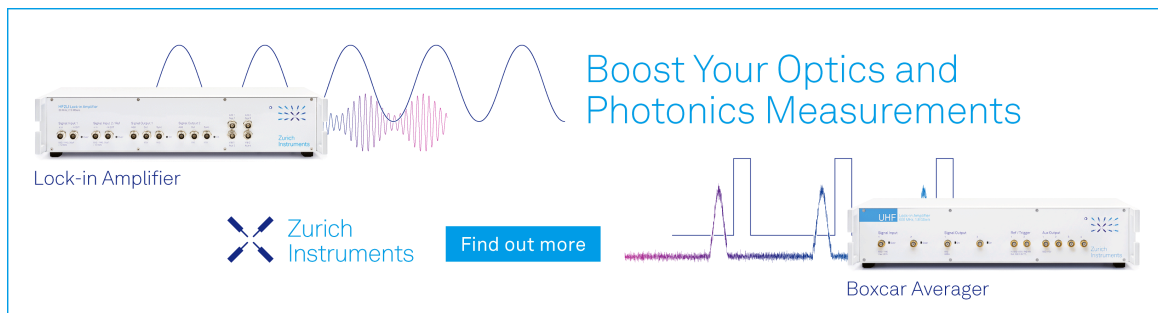
 Check for updates



Appl. Phys. Lett. 124, 212901 (2024)

<https://doi.org/10.1063/5.0211318>



Boost Your Optics and Photonics Measurements



Lock-in Amplifier  [Find out more](#)  Boxcar Averager

Temperature-dependent characterization of full tensor properties of $[111]_c$ poled Mn-doped 28PIN-43PMN-29PT single crystals

Cite as: Appl. Phys. Lett. **124**, 212901 (2024); doi: [10.1063/5.0211318](https://doi.org/10.1063/5.0211318)

Submitted: 29 March 2024 · Accepted: 15 May 2024 ·

Published Online: 22 May 2024



View Online



Export Citation



CrossMark

Ailing Xiao,^{1,2} Liguang Tang,^{1,2,3,a)}  Guisheng Xu,^{4,a)}  Kechen Wu,² and Wenyu Luo³

AFFILIATIONS

¹Key Laboratory of Underwater Acoustic Communication and Marine Information Technology, Ministry of Education, College of Ocean and Earth Sciences, Xiamen University, Xiamen 361010, China

²Fujian Key Laboratory of Functional Marine Sensing Materials, Minjiang University, Fuzhou 350108, China

³State Key Laboratory of Acoustics, Institute of Acoustics, Chinese Academy of Sciences, Beijing 100190, China

⁴R&D Center of Synthetic Crystals, Shanghai Institute of Ceramics, Chinese Academy of Sciences, Shanghai 201800, China

^{a)}Authors to whom correspondence may be addressed: liguotang@xmu.edu.cn and gshxu@mail.sic.ac.cn

ABSTRACT

The temperature-dependent characterization of full tensor properties of single-domain relaxor-based single crystals (SCs) is important for understanding the influence of temperature on the properties of their multidomain SCs. However, no relevant results have been published because characterization is difficult to achieve using the traditional electric resonance method. In this Letter, the temperature-dependent elastic and piezoelectric properties of single-domain $[111]_c$ poled Mn-doped $28\text{Pb}(\text{In}_{1/2}\text{Nb}_{1/2})\text{O}_3$ - $43\text{Pb}(\text{Mg}_{1/3}\text{Nb}_{2/3})\text{O}_3$ - 29PbTiO_3 SCs were investigated in the range of 20–80 °C by resonant ultrasound spectroscopy (RUS) using a rectangular parallelepiped sample. The temperature-dependent dielectric constants were calculated from the measured capacitances of the sample. The results are self-consistent because they were obtained from the same sample. The elastic constants obtained using the ultrasonic pulse-echo method agree closely with those obtained using RUS. Moreover, the experimental results of electric impedance spectrum agree closely with those simulated using the material constants characterized herein, indicating that the characterization is reliable.

Published under an exclusive license by AIP Publishing. <https://doi.org/10.1063/5.0211318>

The excellent performance of multidomain relaxor-based single crystals (SCs) in piezoelectricity has made them become revolutionary materials. Traditional lead zirconate titanate ceramics (PZT) have already been replaced by them in some advanced commercial medical ultrasound equipment. The application of the first-generation binary relaxor-based SCs has been hampered by their low Curie temperatures (T_c), low rhombohedral-to-tetragonal phase transition temperature (T_{RT}),¹ and poor temperature stability. The second-generation ternary SCs, such as $\text{Pb}(\text{In}_{1/2}\text{Nb}_{1/2})\text{O}_3$ - $\text{Pb}(\text{Mg}_{1/3}\text{Nb}_{2/3})\text{O}_3$ - PbTiO_3 (PIN-PMN-PT), have a higher T_c (0–200 °C) and T_{RT} (120–130 °C) without losing high piezoelectric performance,^{2–4} which makes them more promising for the fabrication of electromechanical devices. Doping techniques are often employed to further improve their comprehensive electromechanical properties. The PIN-PMN-PT SCs have a mechanical quality factor (Q_M) around 180; however, that of the third-generation Mn-doped PIN-PMN-PT (PIN-PMN-PT:Mn) SCs can reach 800.⁵

The SCs with a high Q_M can suppress heat generation to improve temperature stability by reducing mechanical losses.

Though $[111]_c$ poled single-domain SCs are not commonly used to fabricate electromechanical devices, studying them is valuable for the following reasons. First, the performance features of single-domain relaxor-based SCs can partially explain the intrinsic mechanism of the excellent electromechanical performance of their multidomain SC counterparts.^{6,7} Second, designers can choose the optimal direction of polarization to achieve high piezoelectric properties according to the full tensor properties of single-domain relaxor-based SCs. Third, single-domain $[111]_c$ poled SCs possess extremely high piezoelectric constant d_{15} ,^{8–11} which may be highly favorable for designing electromechanical devices.¹²

The electric resonance (ER) method is widely used to investigate the full tensor properties of piezoelectric crystals.¹³ Several samples of different sizes must be used in the ER characterization, which may lead to inconsistent or even seriously wrong results.^{14,15} One reason

for this issue is that the sample processing procedure may change the physical properties. Therefore, sample-to-sample variation cannot be avoided. Resonant ultrasound spectroscopy (RUS) is a good alternative to ER for characterizing piezoelectric crystals with a high Q_M .^{16–20}

ER and RUS are two completely different techniques. Xiao *et al.*²¹ compared them in depth. The principle of ER is to determine the elastic and piezoelectric properties (EPPs) from the measured electric resonance and antiresonance frequencies of samples. The RUS technique uses an inversion procedure to study the EPPs based on the ultrasonic resonance frequencies of the sample. RUS is superior to ER when they are used in the temperature-dependent characterization (TDC) of EPPs of piezoelectric crystals. Although RUS is easier to implement than ER, the results obtained by RUS may be more accurate, as illustrated in Ref. 21.

The TDC of the full tensor properties of single-domain relaxor-based SCs is important for understanding the influence of temperature on the material properties of multidomain SCs. However, there are no published results on the TDC of the EPPs of single-domain relaxor-based SCs. In this Letter, the TDC of EPPs of single-domain $[111]_c$ poled 28PIN-43PMN-29PT:Mn SCs with 3m symmetry were conducted from 20 to 80 °C using RUS. The procedure may be extremely complex when ER is used to characterize them, because eight samples of different sizes are needed. Moreover, obtaining reliable results with high precision using ER is difficult.

In this Letter, the x -, y -, and z -axes of the $[111]_c$ poled 28PIN-43PMN-29PT:Mn SC rectangular block sample correspond to the crystallographic directions $[1\bar{1}0]_c$, $[11\bar{2}]_c$, and $[111]_c$, respectively, which has a 3m symmetry.⁵ Its elastic, piezoelectric, and dielectric properties are defined as

$$\mathbf{c}^E = \begin{bmatrix} c_{11}^E & c_{12}^E & c_{13}^E & c_{14}^E & 0 & 0 \\ c_{12}^E & c_{11}^E & c_{13}^E & -c_{14}^E & 0 & 0 \\ c_{13}^E & c_{13}^E & c_{33}^E & 0 & 0 & 0 \\ c_{14}^E & -c_{14}^E & 0 & c_{44}^E & 0 & 0 \\ 0 & 0 & 0 & 0 & c_{44}^E & c_{14}^E \\ 0 & 0 & 0 & 0 & c_{14}^E & c_{66}^E \end{bmatrix}, \quad (1)$$

$$\mathbf{e} = \begin{bmatrix} 0 & 0 & 0 & 0 & e_{15} & -e_{22} \\ -e_{22} & e_{22} & 0 & e_{15} & 0 & 0 \\ e_{31} & e_{31} & e_{33} & 0 & 0 & 0 \end{bmatrix}, \quad (2)$$

and

TABLE I. Measured phase velocities and the related elastic constants for $[111]_c$ poled 28PIN-43PMN-29PT:Mn single crystal.

Wave	$\mathbf{L}^{[1\bar{1}0]}$	$\mathbf{T}_{[111]}^{[1\bar{1}0]}$	$\mathbf{T}_{[112]}^{[1\bar{1}0]}$	$\mathbf{QU}^{[11\bar{2}]}$	$\mathbf{QT}_{[111]}^{[11\bar{2}]}$	$\mathbf{T}_{[1\bar{1}0]}^{[112]}$	$\mathbf{L}^{[111]}$	$\mathbf{T}_{[112]}^{[111]}$
v (m/s)	4875	2936	2315	4929	2509	2706	5027	1311
Elastic constants	c_{11}^E	c_1	c_2	c_3	c_4	c_{66}^E	c_{33}^D	c_{44}^E
c_{ij} (UPE)	19.41	7.044	4.379	19.85	5.144	5.984	20.65	...
c_{ij} (RUS)	19.37	7.086	4.431	19.83	5.348	5.902	20.94	...
Relative deviation	0.21%	0.59%	1.18%	0.10%	3.89%	1.38%	1.39%	...

$$\boldsymbol{\varepsilon}^S = \begin{bmatrix} \varepsilon_{11}^S & 0 & 0 \\ 0 & \varepsilon_{11}^S & 0 \\ 0 & 0 & \varepsilon_{33}^S \end{bmatrix}, \quad (3)$$

respectively, where $c_{66}^E = (c_{11}^E - c_{12}^E)/2$.

The $[111]_c$ poled 28PIN-43PMN-29PT:Mn SC rectangular block sample was obtained from a PIN-PMN-PT crystal boule with an Mn dopant content of 1.0 mol. %, which was grown along the $\langle 111 \rangle$ direction using the modified Bridgman technique. The dimensions of the sample were $4.992 \times 4.890 \times 5.558 \text{ mm}^3$, which were measured using a Mikrometry DHG-050 digital micrometer. The dimension of each direction was obtained from the average of ten measuring points. The standard deviations corresponding to three dimensions were approximately 0.002. Moreover, the density of the sample measured using the Archimedes' method (XF-120MD electronic densitometer) was 8171 kg/m^3 . Ultrasonic pulse-echo (UPE) measurements were performed to obtain several elastic constants. Table I lists the measured phase velocities of different waves and the related elastic constants of the sample, where L, T, QL, and QT in the first row represent the longitudinal, transverse, quasi-longitudinal, and quasi-transverse waves, respectively; the superscripts $[1\bar{1}0]$, $[11\bar{2}]$, and $[111]$ represent the wave propagation directions; and the subscripts $[1\bar{1}0]$ and $[11\bar{2}]$ represent the directions of particle vibration. The elastic constants c_1 , c_2 , c_3 , and c_4 are formulated as^{8,22}

$$c_1 = \frac{c_{44}^D + c_{66}^D + \sqrt{(c_{44}^D - c_{66}^D)^2 + 4(c_{14}^D)^2}}{2}, \quad (4)$$

$$c_2 = \frac{c_{44}^D + c_{66}^D - \sqrt{(c_{44}^D - c_{66}^D)^2 + 4(c_{14}^D)^2}}{2}, \quad (5)$$

$$c_3 = \frac{c_{44}^D + c_{11}^F + \sqrt{(c_{44}^D - c_{11}^F)^2 + 4(c_{14}^D)^2}}{2}, \quad (6)$$

and

$$c_4 = \frac{c_{44}^D + c_{11}^F - \sqrt{(c_{44}^D - c_{11}^F)^2 + 4(c_{14}^D)^2}}{2}, \quad (7)$$

where $c_{11}^F = c_{11}^E + e_{22}^2/\varepsilon_{11}^S$.

The dielectric constants of the SC sample at different temperatures were determined using an HP 4194A impedance analyzer connected to a dielectric temperature spectrum measuring system (Bailibo DMS 2000), as illustrated in Fig. 1.

Figure 2 illustrates the RUS test system, which mainly consisted of a computer, lock-in amplifier (Stanford SR865A), power amplifier (NF HSA4011), environmental chamber (Kingjo Lk-150T), and two

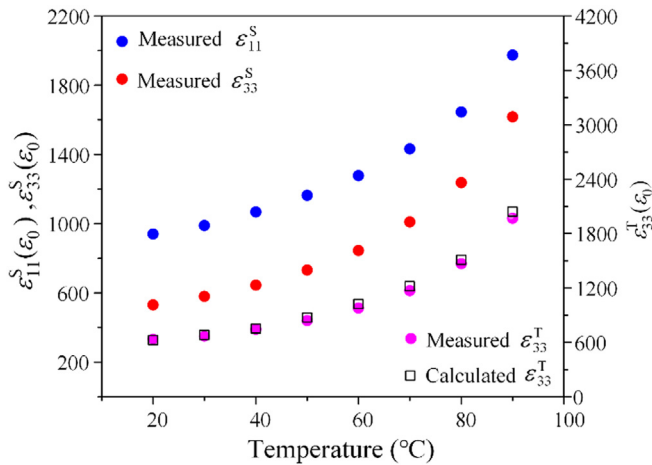


FIG. 1. Temperature dependence of dielectric constants.

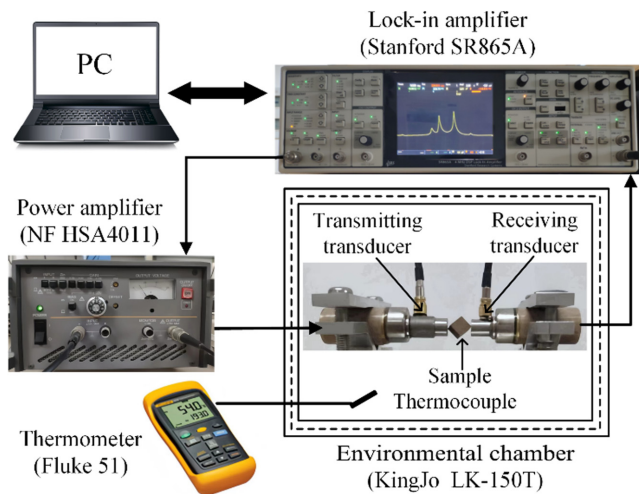


FIG. 2. RUS setup.

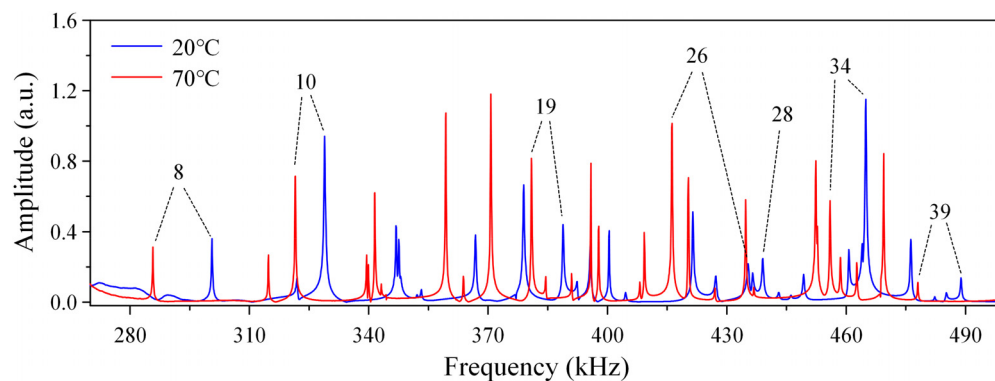


FIG. 3. Resonant ultrasound spectra from 270 to 500 kHz at 20 and 70 °C.

PbNb₂O₆ transducers. The Curie temperature (T_c) of PbNb₂O₆ ceramics was approximately 530 °C, and these systems can maintain good piezoelectric properties under $T_c/2$.²³ During the measurement, two opposite corners of the sample were clamped by the transmitting and receiving transducers. The transmitting transducer was fixed. To protect the sample, the receiving transducer was placed on a slide and connected with a spring. The thermal expansion of the sample will cause the receiving transducer to move on the slide with a very small displacement. Simultaneously, the spring will excite a force on the transducer that will be transferred to the sample such that the sample will not be dropped. If both the transmitting and receiving transducers were fixed, the sample would be broken during thermal expansion.

The resonant ultrasound spectra were measured in the frequency range of 50–800 kHz from 20 to 80 °C. Figure 3 illustrates the typical resonant ultrasound spectra of the SC sample at 20 and 70 °C from 270 to 500 kHz. Note the sample clamping status has great influence on the amplitudes of resonance peaks in the spectra.

Figure 3 illustrates that the resonance frequencies of the [111]_c poled 28PIN-43PMN-29PT:Mn SC sample are highly temperature dependent. All identified resonance frequencies decreased with increasing temperature within the temperature range of 20–80 °C. As the temperature increased, the amplitudes of nearly all the resonance modes changed. Several resonance peaks observed in the spectrum corresponding to temperature T_1 may disappear in the spectrum corresponding to temperature T_2 . For example, resonance modes 11, 28, and 47 are omitted from the spectra at 50, 70, and 60 °C, respectively, as illustrated in Fig. 4. The resonance modes used in the inversion should be sufficient to ensure reliable inversion and obtain accurate results. In this Letter, the omitted modes at a given temperature point were predicted by fitting their temperature-dependent curves using a fourth-order polynomial function based on the measured resonance frequencies. For example, the resonance frequencies corresponding to mode 11 at 50 °C, mode 28 at 70 °C, and mode 47 at 60 °C were predicted using this method, as illustrated in Fig. 4. In the RUS inversion, a total of 85 resonance frequencies were employed, as listed in Table II.

The accurate identification of resonance modes is the most challenging step in RUS. The identification of resonance modes from the spectra at temperature $T + \Delta T$ is easily carried out if sufficient modes are already identified from the spectrum at temperature T because the variation in resonance frequencies is small and predictable if the

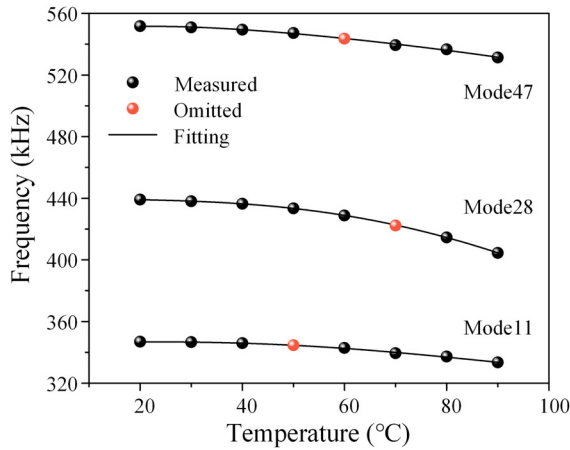


FIG. 4. Temperature dependence of resonance frequencies corresponding to modes 11, 28, and 47.

temperature step ΔT is reasonable. Therefore, a reliable mode identification at room temperature is the basis for mode identification at higher temperatures. To achieve this, the resonant ultrasound spectra were measured repeatedly by changing the sample position. The number of omitted modes can be reduced by comparing the spectra measured under different conditions. In addition, a comparison between the calculated and measured resonance frequencies is indispensable for mode identification. Therefore, reasonable prior information on the full tensor constants at room temperature is necessary for reasonable calculations. Several elastic constants can be determined using the UPE method, as illustrated in Table I.

The determination of the material constants from the identified resonance frequencies of the sample is called the backward problem of RUS. Some solving algorithms of the RUS backward problem can be found in Ref. 24. Figures 5(a)–5(f) illustrate the obtained results for the temperature-dependent elastic stiffness constants $\{c_{11}^E, c_{12}^E, c_{13}^E, c_{14}^E, c_{33}^E, c_{44}^E\}$. Figures 5(g)–5(j) illustrate the obtained results for the

TABLE II. Measured frequencies f_{meas} and calculated resonance frequencies f_{cal} using the constants determined by RUS at 20 °C.

Mode	f_{meas} (kHz)	f_{cal} (kHz)	Diff ^a	Mode	f_{meas} (kHz)	f_{cal} (kHz)	Diff	Mode	f_{meas} (kHz)	f_{cal} (kHz)	Diff
1	96.401	95.272	1.18	31	449.310	448.454	0.19	61	610.652	610.145	0.08
2	196.703	196.777	0.04	32	460.696	459.163	0.33	62	613.829	614.913	0.18
3	232.423	230.473	0.84	33	464.073	463.550	0.11	63	620.045	618.083	0.32
4	254.106	253.952	0.06	34	464.938	465.979	0.22	64	621.244	623.120	0.30
5	259.213	259.180	0.01	35	475.328	474.807	0.11	65	623.669	626.792	0.50
6	261.111	260.172	0.36	36	476.240	477.189	0.20	66	632.478	628.273	0.67
7	263.818	263.863	0.02	37	482.296	482.452	0.03	67	638.359	638.347	0.00
8	300.598	301.589	0.33	38	485.198	485.309	0.02	68	641.203	642.796	0.25
9	321.918	320.767	0.36	39	488.882	486.269	0.54	69	645.495	645.234	0.04
10	328.923	328.241	0.21	40	514.416	514.904	0.09	70	646.053	647.158	0.17
11	346.839	347.127	0.08	41	527.281	528.630	0.26	71	650.290	649.009	0.20
12	347.564	347.773	0.06	42	535.764	534.089	0.31	72	654.081	654.196	0.02
13	347.983	348.582	0.17	43	538.164	539.345	0.22	73	656.980	655.275	0.26
14	352.141	351.948	0.05	44	539.587	540.814	0.23	74	657.760	655.750	0.31
15	353.229	353.663	0.12	45	543.550	543.464	0.02	75	662.611	664.229	0.24
16	366.848	366.093	0.21	46	548.824	549.888	0.19	76	668.241	669.343	0.16
17	376.698	377.237	0.14	47	551.671	550.851	0.15	77	669.774	671.874	0.31
18	378.959	378.470	0.13	48	554.545	554.676	0.02	78	671.531	672.638	0.16
19	388.866	388.354	0.13	49	558.898	558.346	0.10	79	677.329	678.677	0.20
20	50	560.936	560.589	0.06	80	684.604	684.551	0.01
21	51	563.503	562.504	0.18	81	688.395	688.611	0.03
22	400.447	400.481	0.01	52	569.028	567.437	0.28	82	691.155	694.913	0.54
23	404.605	404.611	0.00	53	584.198	585.559	0.23	83	694.583	696.415	0.26
24	421.460	421.727	0.06	54	586.233	585.913	0.05	84	695.698	698.641	0.42
25	427.265	428.418	0.27	55	590.944	591.916	0.16	85	699.768	699.819	0.01
26	435.329	435.364	0.01	56	595.627	595.415	0.04	86	702.305	703.156	0.12
27	436.474	436.264	0.05	57	601.007	600.432	0.10	87	711.308	712.640	0.19
28	439.069	438.963	0.02	58	88	713.650	713.562	0.01
29	443.059	443.002	0.01	59	603.543	603.961	0.07				
30	446.129	444.395	0.39	60	605.049	606.447	0.23				

^adiff = $\frac{|f_{meas} - f_{cal}|}{(f_{meas} + f_{cal})/2} \times 100$.

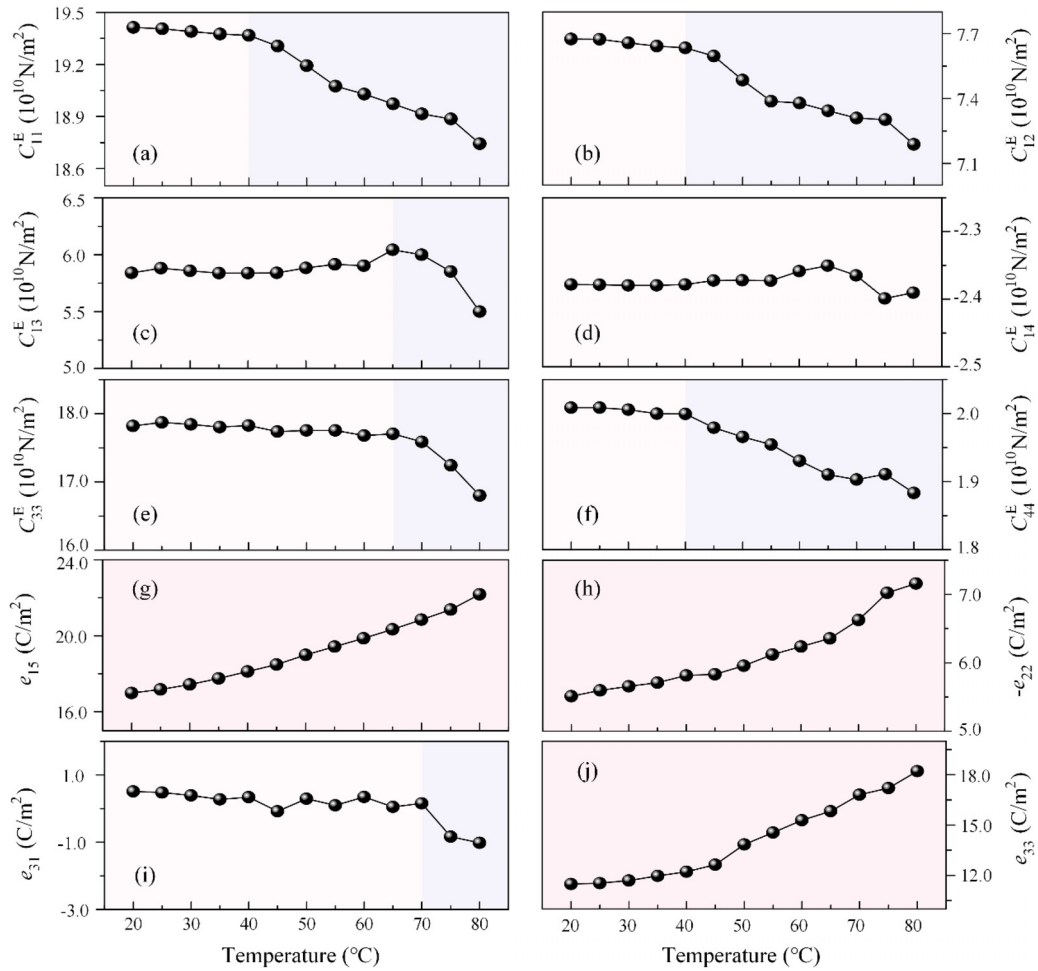


FIG. 5. Temperature dependence of the elastic stiffness constants (a) c_{11}^E , (b) c_{12}^E , (c) c_{13}^E , (d) c_{14}^E , (e) c_{33}^E , and (f) c_{44}^E and piezoelectric stress constants (g) e_{15} , (h) e_{22} , (i) e_{31} , and (j) e_{33} .

temperature-dependent piezoelectric stress constants $\{e_{15}, e_{22}, e_{31}, e_{33}\}$. The elastic constants c_{11}^E , c_{12}^E , and c_{44}^E decrease slowly with increasing temperature in the range of 20–40 °C, as illustrated in Figs. 5(a), 5(b), and 5(f), respectively, showing corresponding reductions of 0.23%, 0.54%, and 0.46%. However, in the range of 40–80 °C, they decrease significantly with increasing temperature; c_{11}^E , c_{12}^E , and c_{44}^E are reduced by 3.23%, 5.85%, and 5.80%, respectively. The elastic constants c_{13}^E , c_{14}^E , and c_{33}^E exhibit good temperature stability between 20 and 65 °C, as illustrated in Figs. 5(c)–5(e), respectively. However, c_{13}^E and c_{33}^E decrease by 9.01% and 5.12%, respectively, from 65 to 80 °C, showing a significant decrease with increasing temperature. Overall, in the range of 20–80 °C, the piezoelectric constants e_{15} , e_{22} (absolute value), and e_{33} increase with increasing temperature, as illustrated in Figs. 5(g), 5(h), and 5(j), respectively. e_{15} , e_{33} , and the absolute value of e_{22} increase by 30.65%, 58.68%, and 29.93%, respectively. Moreover, they vary almost linearly with temperature. The values of the piezoelectric strain constants $\{d_{15}, d_{22}, d_{31}, d_{33}\}$ were obtained using $\mathbf{d} = \mathbf{e}\mathbf{s}^E$, as illustrated in Table III, where \mathbf{d} , \mathbf{e} , and \mathbf{s}^E are the piezoelectric strain, piezoelectric stress,

and elastic compliance matrices, respectively. In the range of 20–80 °C, d_{15} , d_{33} , and the absolute values of d_{22} and d_{31} increase with increasing temperature.

The value of e_{33}^T can be calculated using

$$e_{33}^T = e_{33}^S + 2e_{31}^2(s_{11}^E + s_{12}^E) + 4e_{31}e_{33}s_{13}^E + e_{33}^2s_{33}^E, \quad (8)$$

where the values of elastic compliance constants s_{11}^E , s_{12}^E , s_{13}^E , and s_{33}^E are obtained through inverting the elastic stiffness matrix. The

TABLE III. Temperature dependence of piezoelectric strain constants $\{d_{15}, d_{22}, d_{31}, d_{33}\}$ (units: 10^{-12} C/N).

	20 °C	30 °C	40 °C	50 °C	60 °C	70 °C	80 °C
d_{15}	1838	1895	1978	2130	2295	2506	2812
d_{22}	−419	−432	−450	−482	−518	−567	−643
d_{31}	−14.0	−14.9	−15.8	−18.9	−21.2	−25.2	−31.2
d_{33}	73.5	75.3	78.9	90.5	101	113	129

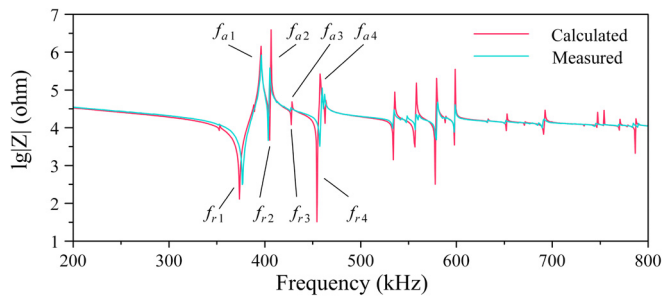


FIG. 6. Electrical impedance spectra measured by the impedance analyzer and calculated by FEM using the RUS results from 200 to 800 kHz at 20 °C.

calculated results agree closely with the experimental values. The relative deviations are less than 4.39% in the 20–80 °C range, which confirms the characterization accuracy of the constants shown on the right side of Eq. (8).

The electrical impedance spectrum of the SC sample at 20 °C was simulated using the EPPs illustrated in Fig. 5 and the dielectric constants illustrated in Fig. 1 with the commercial finite element (FE) software ABAQUS. The results agree well with the measured electrical impedance spectrum, as illustrated in Fig. 6, indicating the TDC reliability of the material constants of the $[111]_c$ poled 28PIN-43PMN-29PT:Mn single crystal. The relative deviations corresponding to the experimental and simulated results of the electric resonance frequencies f_{r1} , f_{r2} , f_{r3} , and f_{r4} , as illustrated in Fig. 6, are less than 0.83%. The relative deviations corresponding to the experimental and simulated results of the electric antiresonance frequencies f_{a1} , f_{a2} , f_{a3} , and f_{a4} are less than 0.50%, as illustrated in Fig. 6.

In summary, the TDC of the elastic, piezoelectric, and dielectric properties of the single-domain $[111]_c$ poled 28PIN-43PMN-29PT:Mn SCs were conducted in the temperature range of 20–80 °C. The dielectric constants ϵ_{11}^S and ϵ_{33}^S were obtained from the measured capacitances of the SC sample. The temperature-dependent elastic stiffness constants $\{c_{11}^E, c_{12}^E, c_{13}^E, c_{14}^E, c_{33}^E, c_{44}^E\}$ and piezoelectric stress constants $\{e_{15}, e_{22}, e_{31}, e_{33}\}$ were obtained using RUS. The results are self-consistent because they were characterized from the same SC sample. The elastic constants c_{11}^E , c_{66}^E , and c_{33}^D determined using RUS agree closely with those obtained using UPE. The electric impedance spectrum calculated using the material constants obtained in this study is consistent with the measured spectrum, indicating that the characterization results are reliable. In our future work, the TDC of the full tensor constants of multidomain $[001]_c$ poled PIN-PMN-PT:Mn SCs will be conducted and compared with the results obtained in this Letter to investigate the influence of temperature on the piezoelectric properties of multidomain SCs.

This work was supported by the National Natural Science Foundation of China (Grant No. 12274358), the State Key Laboratory of Acoustics, Chinese Academy of Science (Grant No. SKLA202309), the Fujian Key Laboratory of Functional Marine Sensing Materials, Minjiang University (No. MJUKF-FMSM202207), and the Leading Special Project of the Chinese Academy of Sciences (Grant No. XDA25020312).

AUTHOR DECLARATIONS

Conflict of Interest

The authors have no conflicts to disclose.

Author Contributions

Ailing Xiao: Data curation (equal); Formal analysis (equal); Investigation (equal); Writing – original draft (supporting); Writing – review & editing (equal). **Liguo Tang:** Conceptualization (equal); Data curation (equal); Formal analysis (equal); Funding acquisition (equal); Project administration (equal); Resources (equal); Supervision (equal); Writing – review & editing (equal). **Guisheng Xu:** Conceptualization (equal); Investigation (equal); Resources (equal); Supervision (equal); Writing – review & editing (equal). **Kechen Wu:** Funding acquisition (equal); Resources (supporting). **Wenyu Luo:** Resources (equal).

DATA AVAILABILITY

The data that support the findings of this study are available from the corresponding authors upon reasonable request.

REFERENCES

- Tian and P. D. Han, *Crystals* **4**(3), 331–341 (2014).
- J. Zhang, J. Luo, W. Hackenberger, and T. R. Shrout, *J. Appl. Phys.* **104**(6), 064106 (2008).
- Tian, P. D. Han, X. L. Huang, and H. X. Pan, *Appl. Phys. Lett.* **91**(22), 222903 (2007).
- S. J. Zhang, J. Luo, W. Hackenberger, N. P. Sherlock, R. J. Meyer, Jr., and T. R. Shrout, *J. Appl. Phys.* **105**(10), 104506 (2009).
- S. J. Zhang, F. Li, X. N. Jiang, J. W. Kim, J. Luo, and X. C. Geng, *Prog. Mater. Sci.* **68**, 1–66 (2015).
- X. Z. Liu, S. J. Zhang, J. Luo, T. R. Shrout, and W. W. Cao, *Appl. Phys. Lett.* **96**(1), 012907 (2010).
- X. Z. Liu, S. J. Zhang, J. Luo, T. R. Shrout, and W. W. Cao, *Appl. Phys. Lett.* **97**, 019901 (2010).
- R. Zhang, B. Jiang, and W. W. Cao, *Appl. Phys. Lett.* **82**(5), 787–789 (2003).
- P. D. Han, W. L. Yan, J. Tian, X. L. Huang, and H. X. Pan, *Appl. Phys. Lett.* **86**(5), 052902 (2005).
- S. F. Liu, W. Ren, B. K. Mukherjee, S. J. Zhang, T. R. Shrout, P. W. Rehrig, and W. S. Hackenberger, *Appl. Phys. Lett.* **83**(14), 2886–2888 (2003).
- M. Davis, M. Budimir, D. Damjanovic, and N. Setter, *J. Appl. Phys.* **101**(5), 054112 (2007).
- F. Li, S. J. Zhang, J. Luo, X. C. Geng, Z. Xu, and T. R. Shrout, *J. Appl. Phys.* **120**(7), 074105 (2016).
- The Institute of Electrical and Electronics Engineers, Inc., “IEEE standard on piezoelectricity,” Standard No. 176-1987 (ANSI/IEEE, 1988).
- M. Shanthi, L. C. Lim, K. K. Rajan, and J. Jin, *Appl. Phys. Lett.* **92**(14), 142906 (2008).
- Y. Y. Topolov, *Appl. Phys. Lett.* **96**(19), 196101 (2010).
- R. Tarumi, T. Matsuhisa, and Y. Shibutani, *Jpn. J. Appl. Phys., Part 1* **51**, 07GA02 (2012).
- L. G. Tang and W. W. Cao, *Appl. Phys. Lett.* **106**(5), 052902 (2015).
- L. G. Tang, H. Tian, Y. Zhang, and W. W. Cao, *Appl. Phys. Lett.* **108**(8), 082901 (2016).
- J. Hu, H. T. Fan, S. J. Wu, L. G. Tang, L. Qin, and W. W. Luo, *Ceram. Int.* **48**(18), 25741–25746 (2022).
- N. G. Fenu, N. Giles-Donovan, M. R. Sadiq, and S. Cochran, *IEEE Trans. Ultrason., Ferroelectr. Freq. Control* **68**(5), 1797–1807 (2021).
- A. L. Xiao, L. G. Tang, S. S. Sun, S. J. Wu, X. Y. Wu, and W. Y. Luo, *IEEE Trans. Instrum. Meas.* **72**, 6007915 (2023).
- C. W. Chen, Y. Xiang, L. G. Tang, X. W. Li, L. Qin, and W. W. Cao, *J. Mater. Sci.* **55**(27), 12737–12746 (2020).
- R. Q. Jin, X. D. Ren, L. Q. Hu, M. Y. Tang, Z. Xu, and Y. K. Yan, *J. Am. Ceram. Soc.* **107**(7), 4914–4924 (2024).
- J. Pujol, *Geophysics* **72**(4), W1–W16 (2007).